Journal of the Brazilian Society of Mechanical Sciences and Engineering (2024) 46:572
https://doi.org/10.1007/s40430-024-05144-x

TECHNICAL PAPER

Comprehensive exploration of technological tensioning effects in welded thin plate girders: an in-depth investigation

Hassanein I. Khalaf[1] · D. Chodorowska[2] · Raheem Al-Sabur[1] · Andrzej Kubit[3] · Wojciech Macek[4]

Received: 14 February 2024 / Accepted: 12 August 2024

Abstract

Thin-walled plate girders are widely used in structures and construction due to their effectiveness in transferring loads. The permanent deformations of the girder lead to a lack of stability, which necessarily leads to its replacement. Replacing permanently deformed thin-walled load-bearing structures requires large financial outlays. Technological prestressing is one of the most effective methods for studying and treating permanent deflections in girder elements. This study looks at the defection of welded thin-plate S235JR steel girders, examining how technological tensioning effects interact with different loading conditions. Four girders, A2 (welded in bottom caps), A3 (welded in two side caps), and A4 (welded in two side caps and bottom caps), as well as the prestressed B2 girder, which has two welded side caps, were subjected to a bend test. The girders were subjected to a load P (20, 40, 60, 80 and 95) kN. All points were examined during the 95 min of cooling time. For technological compression, the results showed that there is a convergence between the analytical solution and the experimental results, as the most significant deviation achieved in the analysis was 5.21 mm compared to 6 mm experimentally. When the girder is loaded with the force $P = 50$ N, the maximum deflection achieved at girder A4 is 4 mm, compared with 1mm at girder A2. In prestressed girder B, the deflections that were reached were 2.50 mm, 3.50 mm, and 3.52 mm in the analytical, experimental, and FE numerical models, respectively. The tensions that were reached were 36.96 MPa, 44.28 MPa, and 27.93 MPa.

Keywords Thin plate girder · Technological tensioning · Defection · Prestress · Technological compression

1 Introduction

Girders are of sound importance to structures and construction due to their efficiency in carrying loads [1, 2]. The girders are still the subject of extensive research and investment [3]. Bridges, including highways, industrial structures, buildings, and even aerospace structures, are typical applications of thin-walled plate girders [4]. Thin-walled plate girders and box girders are the main types of industrial girders [5].

As a result of the extended operation of load-bearing structures, such as the main load-bearing elements of girders, deformation accelerates to varying degrees [6]. Permanent deflections of girders may manifest in the vertical and horizontal planes, as may deformations of girder cross sections and local web and stability losses [7]. Permanent deformations entail the need to shut down the girders from further use, which in turn causes economic losses or a reduction in production efficiency [8]. The issue's importance is now of great importance as the progressing process of increasing permanent deflections of thin-walled crane girders is observed more and more often in industrial plants.

The reasons for the increase in permanent deflections are complex, and they can be due to overloading that leads to lamellar crack propagation in the girder elements, which develop over time, and the ageing of the material [9]. The

Technical Editor: João Marciano Laredo dos Reis.

✉ Raheem Al-Sabur
raheem.musawel@uobasrah.edu.iq

[1] Mechanical Department, Engineering College, University of Basrah, Basrah, Iraq

[2] The State Higher School of Vocational Education in Krosno, Ul. Wyspiańskiego 20, 38-400 Krosno, Poland

[3] Department of Manufacturing and Production Engineering, Faculty of Mechanical Engineering and Aeronautics, Rzeszow University of Technology, Al. Powst. Warszawy 8, 35-959 Rzeszów, Poland

[4] Faculty of Mechanical Engineering and Ship Technology, Gdańsk University of Technology, 11/12 Gabriela Narutowicza Street, 80-233 Gdańsk, Poland

Published online: 28 August 2024

increase in permanent deflections exhausts the structure's load capacity and, at the same time, affects the proper operation of transport equipment due to the increasing resistance to their movement on the crane bridge and the crane roadway [10]. Replacing permanently deformed thin-walled load-bearing structures (box girders, plate girders) require large financial outlays [11]. Therefore, it becomes necessary to develop an effective regeneration method that will not only eliminate permanent deflections but also positively affect the strength effects caused by the formation of permanent deflections. Technological prestressing is one of the most effective methods for studying and treating permanent deflections in girder elements. It is an original solution related to the strength regeneration of permanent deflections, especially in box girders of crane bridges [12].

The technological prestressing method is characterized by its ability to bend the girder in the horizontal and vertical planes [13]. It depends on the welding shrinkage phenomenon of fillet welds of additional overlay sheets welded to the tension zone caused by the plate girder loads [14]. The introduced welding stresses cause stretching of the compressed area of the structure and compression of the tension zone, which leads to the bend of the girder with upward convexity [15].

Because of its great importance to structural engineering, steel plate girders have remained a fertile field for intensive research. Studies have advanced understanding of plate girders' complex relationship between bending, shear, and buckling phenomena. This study attempts to review an essential aspect of these studies, especially those related to technological tensioning effects in welded thin plate girders.

Hingnekar et al. [16] reviewed the historical development of tension field theories. They investigated the effect of shear loads on the behaviour of steel plate girders. They also showed the importance of post-buckling strength in predicting the ultimate shear resistance of stiffened web panels. Nascimento et al. [17] gave an insight into the behaviour of the plate girder when it was reinforced with intermediate transverse stiffeners, and they showed that this strengthening contributed significantly to limiting lateral panel buckling. Applications of plate girders in seismic-prone areas were the focus of the study by Natesh et al. [18], where they used different loading conditions. They investigated using analysis and modelling of plate girders that the member with a slenderness ratio can provide the most protection possible when it is 150–175 under steady-state loading conditions or the behaviour of beams designed according to elementary beam theory under various loading scenarios. Shawky et al. [19] compared the results obtained using the ANSYS software with the experimental results of two plate girders subjected to post-buckling behaviour. The girder cross section was an I-section with a length of 2.5m. They found that there was good convergence between the experimental results and the numerical results when bending and shear were applied. Despite the in-depth experiments Scandella et al. [20] carried out about the stability of steel-plate girders under shear loading and their conclusion that post-critical behaviour is dual-stage, they concluded the need for additional experimental and numerical studies to give a more precise and more accurate understanding. The effect of stiffener inclination angles on both post-buckling behaviour and load-carrying capacity was studied by Yatim et al. [21]. They indicated that decreasing the angle of inclined stiffeners for steel plate girders shows a noticeable increase in ultimate strength. Cakiroglu et al. [22] concentrated on optimizing the lateral-torsional buckling and shear requirements of steel plate girders employing meta-heuristic algorithms. They presented a creative method for optimizing cross-sectional designs. The steel plate girder's shear failure characteristics excited by Alinia et al. [23] indicated that the shear-induced plastic hinges evolved in the end panels only.

The current body of research on steel plate girders has primarily focused on individual aspects such as shear, buckling behaviour, and stability, often overlooking the intricate effects of technological tensioning processes. An important issue yet to be investigated is assessing the impact of prestressing on the strength of plate girders compared to that of unstressed girders. This problem is essential for the stability of the prestressing plate girders with slender cross sections. So, in the current study, the behaviour of thin plate girders constructed through welding is investigated using analytical, experimental, and numerical approaches focusing on the interplay between the technological effects of stress and bending load.

2 Materials and methods

The experimental model consists of welded plate girders and two supports fixed at both ends on the foundation (ground) designed to withstand forces up to 150 kN. A 20-ton hydraulic jack with a force gauge to measure the jack's pressure force was fixed between the plate girders and the ground. Moreover, two indicator stands were added for more accurate measurement, as shown in Fig. 1. The supporting structures of the girder were made of standard IPE100 I-beams (depth 100 mm, width 55 mm, web 4.1 mm, and flange 5.7 mm) and sheets of $10 \times 340 \times 340$ mm made of S235JR steel. Rods made of 40HGA steel, with a diameter of Ø44 mm and a length of 280 mm, perform the joint's function. In addition, the girder supports consist of sheets made of S235JR steel, to which a shaft with a diameter of Ø44 mm was welded. The whole was initially bolted using M24 × 650 bolts and M24 nuts with washers, then tightened with 120 Nm torque. This robust mounting method ensured that deflection measurements were solely due to the girder itself, eliminating

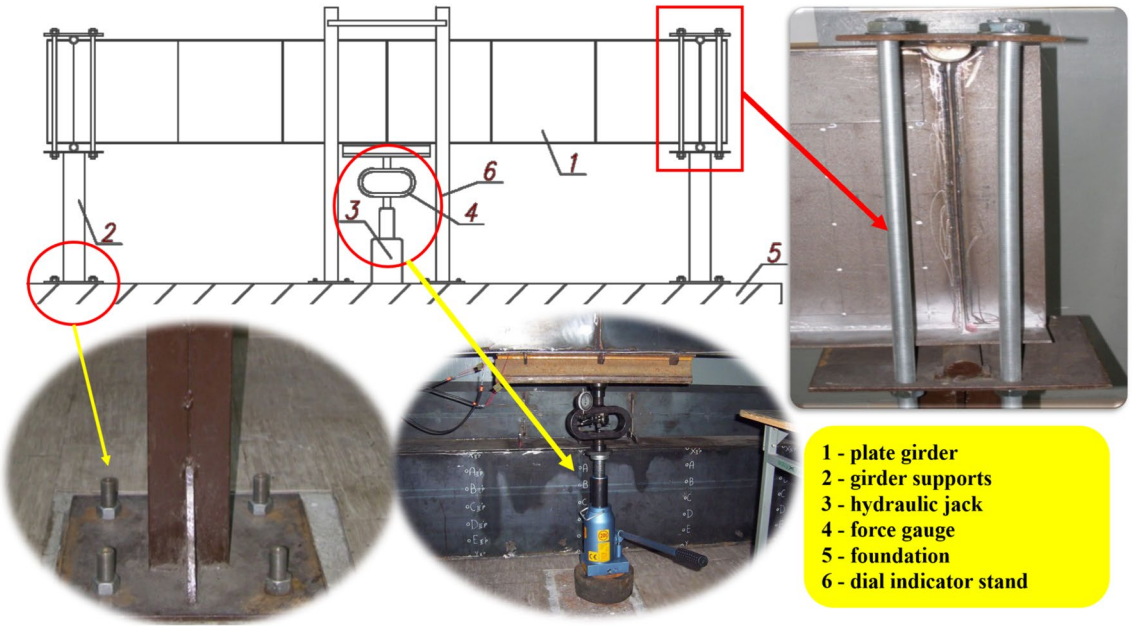

Fig. 1 Experimental model for plate girder study

the possibility of deflection in the supports. The design and assembly of the supporting structures provided a rigid and stable platform, effectively addressing concerns about any potential displacement of the stand.

The girder configuration comprises two sections: girders A and B. Girders A1 and B1 are unstressed. In contrast, the prestressed A girder consists of three parts: A2 (welded in bottom caps), A3 (welded in two side caps), and A4 (welded in two side caps and bottom caps) and the prestressed B2 girder, which are two welded side caps, as shown in Fig. 2.

Three loading types were applied on the thin plate girder: a) uncompressed, loaded with force *P*; b) prestressed, loaded with prestressing forces and moments; and c) prestressed, loaded with prestressing forces and moments and with force *P*.

The experimental model was presented to measure stresses, deflections, and displacements of type A and B girders. The plate girder was rotated at 180° to carry out the process of technological prestressing. Such a girder arrangement ensured the correctness of the welding process and

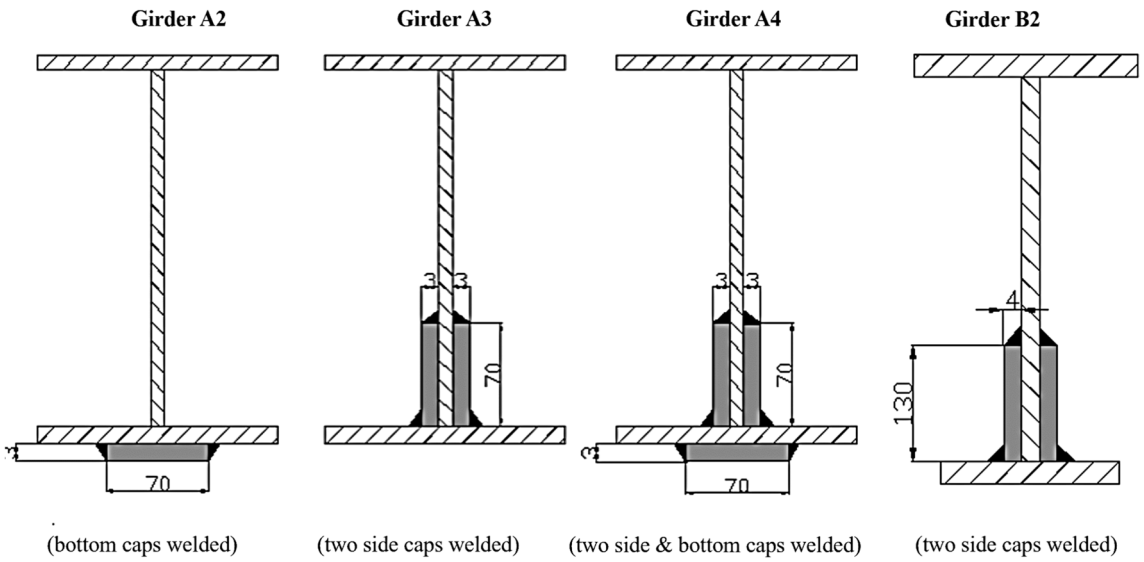

Fig. 2 Thin plate girders A and B welding configurations

minimized weld defects. The side fins should be welded at the bottom of the web, so the stressing process was carried out under conditions reflecting the actual position of the structure. It is worth noting that it is impossible to apply the above load for the measurement tests of the deflection and the stresses before and after the prestressing process. So that the girder model was inverted so that the force was applied from below, while the side caps were in the upper part of the web. Such a location of the plate girder during the tests did not affect the results obtained. Stresses, due to the self-weight of the structure, do not exceed the value of 0.8 MPa. The analytical calculations considered the fact that the girder was loaded from below.

The stress measurement was taken and presented for type B girders. HBM 10/120LY41 Hottinger strain gauges measure the stresses of an unstressed plate girder loaded with the force P. The strain gauges have a resistance of 120 Ω, sensitivity factor $k = 2.1$. Z-70 glue was used for glueing, and the sensors were protected against high temperatures with AK-75 putty by Hottinger. All measuring sensors (Fig. 3) had their compensation strain gauges glued on a plate of the same type as the girder and attached near the measuring sensor, allowing maximum compensation of the influence of temperature. Figure 4 indicates shows the sensor's position on the girder after the technological prestressing process. For the correct operation of the compensation sensor, the plate was mounted using a special heat-conducting silicone paste and mounting silicone resistant to temperatures up to 3500C. Then, all measuring, and compensation sensors were connected through a distribution box into a half-bridge system using mounting cables in the LIYCY 2×0.34 mm2 screen and connected to the UPM-100 strain gauge bridge coupled with a PC.

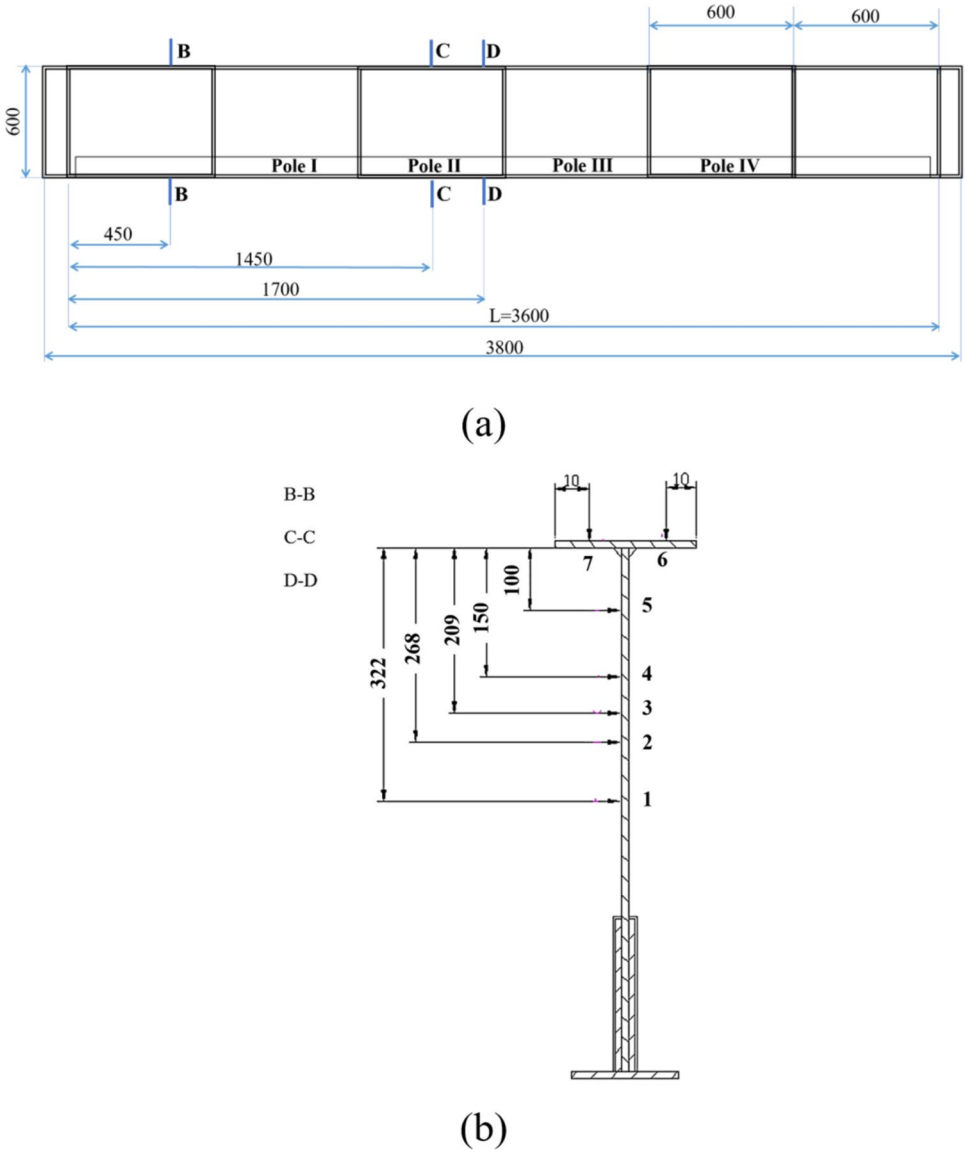

Fig. 3 **a** Thin plate girders sections and **b** locations of measurement points [all dimensions in mm]

Fig. 4 Sensor's position on the girder after the technological prestressing process

3 Theory and methodology

An external load causes a non-uniform axial stress state in the structure (bending with compression or bending with tension). Knowing the locations of the measured points (stress values) on this plane, as shown in Fig. 3b, is sufficient to characterize the stress state plane, which is shaped in this way and is inclined to the section plane. The stress values as a function of the axial force and the components of the bending moments are described by the following relationships:

$$\sigma_i = \frac{N}{A} + \frac{M_x}{I_{xg}} \cdot y_i + \frac{My}{I_{yg}} \cdot x_i$$

$$\sigma_j = \frac{N}{A} + \frac{M_x}{I_{xg}} \cdot y_j + \frac{My}{I_{yg}} \cdot x_j \tag{1}$$

$$\sigma_k = \frac{N}{A} + \frac{M_x}{I_{xg}} \cdot y_k + \frac{My}{I_{yg}} \cdot x_k$$

where N, M_x, and M_y appropriate values of the axial force of the bending moment M_x (w central plane), M_y (w main plane yz), σ_i, σ_j, and σ_k are stress values at given points i, j, k. I_{xg}, I_{yg} are main central moments of inertia, A-bar cross-sectional area, E-Young's modulus, $x(i, j, k)$, $y(i, j, k)$ are coordinates of gluing points of tension gauges—thrust w with the main central axes of inertia, the cross section of the bar.

Solving the system of Eqs. (1) about the axis of internal forces N, M_x, and M_y leads to:

$$F = A \cdot \frac{\sigma_i \cdot (x_k \cdot y_j - x_j \cdot y_k) + \sigma_j \cdot (x_i \cdot y_k - x_k \cdot y_i) + \sigma_k \cdot (x_j \cdot y_i - x_i \cdot y_j)}{x_i \cdot (y_k - y_j) + x_j \cdot (y_i - y_k) + x_k \cdot (y_j - y_i)}$$

$$M_x = I_{xg} \cdot \frac{\sigma_i \cdot (x_j - x_k) + \sigma_j \cdot (x_k - x_i) + \sigma_k \cdot (x_i - x_j)}{x_i \cdot (y_k - y_j) + x_j \cdot (y_i - y_k) + x_k \cdot (y_j - y_i)} \quad (2)$$

$$M_y = I_{yg} \cdot \frac{\sigma_i \cdot (y_k - y_j) + \sigma_j \cdot (y_i - y_k) + \sigma_k \cdot (y_j - y_i)}{x_i \cdot (y_k - y_j) + x_j \cdot (y_i - y_k) + x_k \cdot (y_j - y_i)}$$

The values of internal forces in the tested cross sections were determined based on the computational transformation of the state of stress to the corresponding state of the components of internal forces. All possible combinations of measurement points were used in the calculation process, taking measurement points 1, 2, 3, 4, 5, 6, and 7 as *i*, *j*, and *k*. Points 6 or 7 were used as control points in each combination. The average calculation results are presented in Table 1.

Despite the significant development in the plate girder design, the analytical solution and the design principles still depend on the fundamental principles laid down by N. O. Okerblom [24]. These principles are based on welding calculations for girder parts to determine the deflection (*f*), prestressed force (Fps), and prestressed moment (Mps) as below:

$$f_i = \frac{C_i \cdot L \cdot l_i}{8}$$

$$\mathrm{HAZ}_{(ax)} = \frac{57,5a^2}{1 + 2\frac{57,5a^2}{A}}$$

$$F_{ps(ax)} = 2 \cdot \sigma y \cdot HAZ_{(ax)} \quad (3)$$

$$M_{ps(ax)} = F_{ps(ax)} \cdot e$$

where HAZ_{ax} is heat effective zone area, a is fillet weld thickness, *and A* is cross-sectional area of the girder.

4 Results and discussion

4.1 Analytical solution of technological compression

Equations 1–3 govern the output of the analytical solution for technological compression; for each girder part, the arc welding energy was calculated, followed by the total deflection of a plate girder and the heat-affected zone area according to the fillet weld thickness dimensions in Fig. 3. Prestressed force (Fps) and prestressed moment (Mps) were calculated from Eq. 2. Table 1 describes the results obtained from the analytical solution.

4.2 Stress measurement of unstressed girder B1

Five loads of P are applied (20, 40, 60, 80, and 95) kN on seven positions of each girder section (A, B, C, and D). The stresses of the unstressed girder of each point that indicated in Fig. 3 were measured. The obtained measurement results, which are the average of three measurements, are summarized in Table 2.

On the other hand, solving Eqs. (3) about the axis of internal forces *N* and moments M_x leads to calculating the internal forces and moments in the tested cross sections. All possible combinations of measurement points were used in the calculation process, taking measurement points 1, 2, 3, 4, 5, 6, and 7 as *i*, *j*, and *k*. Points 6 or 7 were used as control

Table 2 List of measured values of unstressed girder stresses [MPa]

Stress	Girder load with force *P* [kN]				
	20	40	60	80	95
σ_{B1}	0.62	1.64	2.66	3.89	5.12
σ_{B2}	0.82	1.05	2.28	3.15	4.19
σ_{B3}	− 1.64	− 3.48	− 5.12	− 6.70	− 8.40
σ_{B4}	− 2.23	− 5.25	− 7.48	− 9.37	− 10.34
σ_{B5}	− 3.56	− 7.66	− 10.30	− 12.97	− 17.15
σ_{B6}	− 5.80	− 11.90	− 17.90	− 24.09	− 28.74
σ_{B7}	− 5.80	− 11.90	− 17.90	− 24.09	− 28.74
σ_{C1}	1.03	2.46	4.51	6.97	9.02
σ_{C2}	− 0.23	− 0.85	− 1.26	− 1.75	− 1.98
σ_{C4}	− 8.41	− 16.60	− 24.81	− 33.00	− 38.74
σ_{C6}	− 18.65	− 35.46	− 50.43	− 64.57	− 74.21
σ_{C7}	− 18.65	− 35.46	− 50.43	− 64.57	− 74.21
σ_{D1}	5.17	9.14	13.00	20.47	29.18
σ_{D2}	0.46	0.72	1.76	1.98	2.04
σ_{D3}	− 2.66	− 5.53	− 8.61	− 12.09	− 14.76
σ_{D4}	− 7.99	− 16.19	− 24.60	− 33.21	− 39.77
σ_{D6}	− 16.19	− 37.92	− 61.30	− 86.30	− 106.80

Table 1 HAZ area values and deflection arrows obtained by analytical solution

Terms	Girder A2	Girder A3	Girder A4	Girder B2
HAZ area [mm^2]	285.38	289.59	293.33	427.92
Prestressing forces F_{ps} [kN]	134.13	272.20	413.58	402.24
Prestressing moments M_{ps} [kNm]	28.49	44.90	67.50	81.34
Deflection *f* [mm]	1.70	3.25	4.47	2.49

Table 3 Internal forces values in individual sections

Factor	Force P	Section B	Section C	Section D
N [kN]	20 [kN]	− 3.66	− 6.18	− 10.28
	40 [kN]	− 9.10	− 11.09	− 18.17
	60 [kN]	− 13.79	− 14.93	− 27.30
	80 [kN]	− 19.55	− 17.83	− 34.17
	95 [kN]	− 24.60	− 19.08	− 38.47
M_x [kNm]	20 [kN]	1.60	12.13	17.81
	40 [kN]	4.20	24.58	35.61
	60 [kN]	5.60	37.34	53.65
	80 [kN]	8.43	50.37	71.33
	95 [kN]	11.24	60.10	84.59
M_y [kNm]	20 [kN]	0.32	0.01	− 0.21
	40 [kN]	0.53	0.10	− 0.22
	60 [kN]	0.86	0.25	− 0.17
	80 [kN]	1.15	0.42	− 0.06
	95 [kN]	1.34	0.59	0.08

points in each combination. The average calculation results are presented in Table 3.

Results of the internal forces (F, M_x, and M_y) in section B under different applied forces (20, 40, 60, 80, and 95 [kN]) led to more negative (tensile axial force) under increasing applied forces, which indicates that this section is experiencing tension as the applied force increases. The bending moments (M_x and M_y) also grow with higher applied forces. Both M_x and M_y are positive, meaning that this section is undergoing bending in the x and y directions. The magnitudes of the M_x and M_y are proportional to the applied forces, as expected in a linear elastic behaviour. In the other three sections, the general behaviour of internal forces differs significantly from section B. It is worth noting section D experiences more extensive magnitudes of bending moments (M_x and M_y) under the same applied forces. M_x and M_y increase nonlinearly with applied forces, revealing a stiffer response than other sections.

The obtained values of internal forces in Table 2 made it possible to determine the actual conditions for fastening the tested structure, illustrated in Fig. 5. The obtained moment M_x at points B, C, and D led to finding the moment value corresponding to the plate girder fixing point indicated by the dashed line.

4.3 Girder measurements after technological compression process

4.3.1 Girder deflection

After the process of technological stressing was carried out, and the structure cooled down, the value of the girder deflection was measured with the upward convexity in the middle section. The obtained results are summarized in Table 4. The calculated inflection of the girder with upward convexity significantly differed from the outcomes of the calculations made using Okerbom et al. mathematical model [24].

4.3.2 Girder stresses

During the process of technological prestressing, the values of stresses generated in the structure were measured. The measurements were taken for a type B girder. To protect the strain gauges against high temperatures as much as possible, they were additionally covered with aluminium foil. Stress measurements were taken during the compression process

Table 4 Girder deflection arrow after technological prestressing

	Girder A2	Girder A3	Girder A4	Girder B2
Deflection f [mm]	2.90	4.00	6.00	3.50

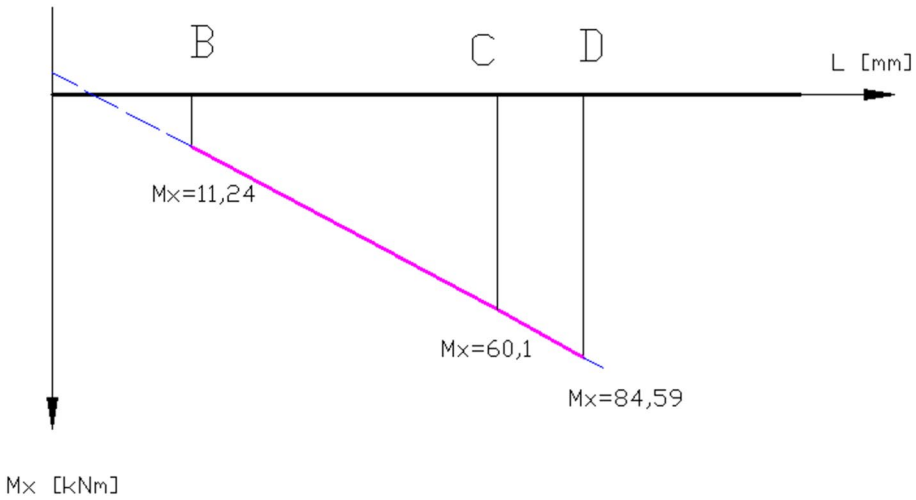

Fig. 5 Analytical bending moment M_x variation concerning plate girder sections

Table 5 Measured stresses values in [MPa]

Stress	Welding	First	Second	minutes After welding				
	Starting	weld	weld	5 min	20 min	35 min	50 min	95 min
σ_{B2}	55.76	33.62	−83.91	−72.59	−89.60	−97.40	−100.67	−102.52
σ_{B6}	−16.61	23.99	−16.81	71.75	35.47	37.93	39.16	39.77
σ_{B7}	−14.61	21.85	−12.72	6.51	30.26	32.46	35.12	35.13
σ_{C4}	18.86	6.36	−13.12	−12.71	−28.50	−29.73	−30.55	−31.16
σ_{C6}	30.96	−26.45	92.05	26.65	30.55	31.98	33.21	33.62
σ_{C7}	24.50	−25.63	25.42	23.06	26.86	28.09	29.00	29.62
σ_{D1}	−66.26	−74.27	28.91	−89.72	−92.77	−95.10	−100.80	−102.61
σ_{D6}	19.25	−21.18	52.13	30.80	42.15	43.98	45.13	45.12
σ_{D7}	21.53	−23.58	51.66	32.80	41.41	44.08	44.49	44.28

and every 15 min after the end of welding until the structure cooled down to ambient temperature. In addition, in sections C3 and C5, continuous stress measurements were recorded. Table 5 presents the stress values for three randomly selected points, for which the stress state was transformed into the corresponding state of the components of internal forces. After the technological compression process was completed, the temperature in the C-C section of the girder was measured using a digital temperature meter.

Figure 6 shows the change of temperature as a function of time in the upper weld in the middle section of the girder. It shows the change of temperature as a function of time in the upper weld in the middle section of the girder.

The values of internal forces were found using Aistow's equations to change the state of stress into the corresponding state of the components of internal forces. This was done by knowing the values of stresses in the structure caused by technological prestressing. The results obtained for the D-D section are shown in Fig. 7.

The analysis of the measurement results and the computational transformation of the state of stress into the corresponding state of the components of internal forces generated in the structure because of the technological prestressing process were performed for sections B, C, and D in a similar way as for the unstressed girder.

The calculation results obtained were averaged and are presented in Table 6. The results in Table 6 agree with the values of the prestressing force and the prestressing moment found through analytical calculations. These values were based on tests of the girders' deflection arrows after the technological prestressing process.

The values of the prestressing forces and moments are a function of the area of the active HAZ area and the yield point of the steel. In the analytical model of [24], the yield strength of welded elements of S235JR steel, $\sigma y = 235$ [MPa], was assumed a priori. To check the accuracy of the computer model for plate girder structures that were made from tests that were done, a static tensile test was done on

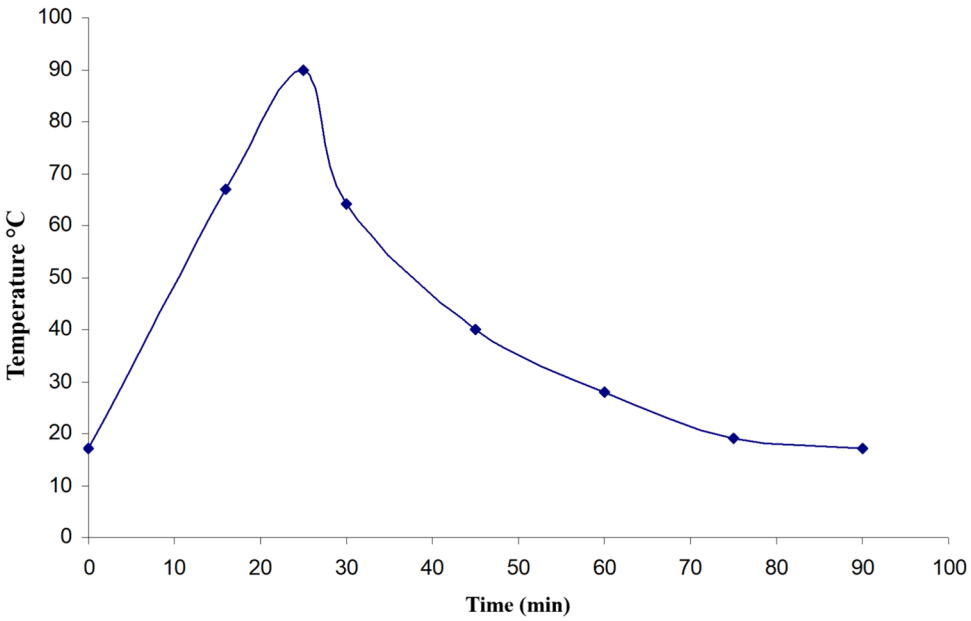

Fig. 6 Temperature distribution as a function of time on the top weld of the girder

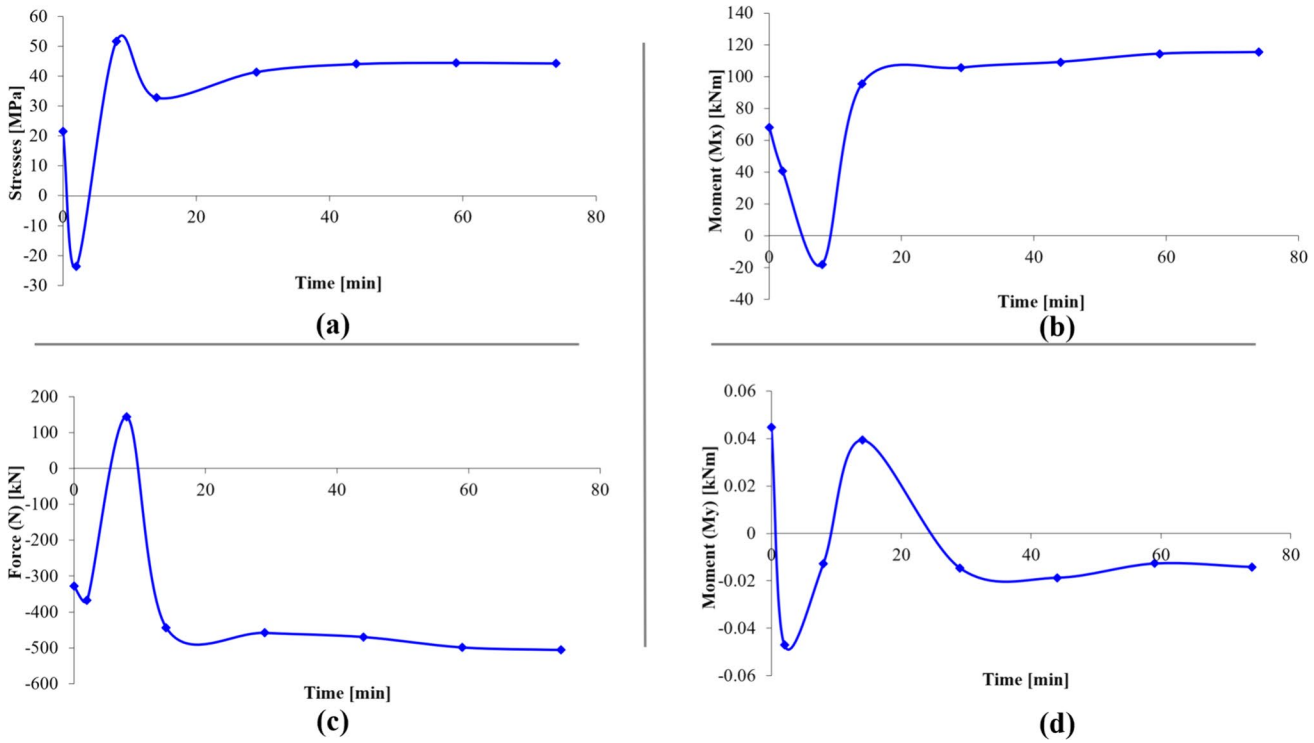

Fig. 7 Variation of **a** stresses, **b** internal force N, **c** moment M_x, and **d** moment M_y versus welding and cooling time in D-D section

Table 6 Average values of internal forces in a plate girder after cooled down to room temperature

	Section B	Section C	Section D	Mean values
N [kN]	−658.08	−495.23	−507.00	−553.43
M_x [kNm]	135.82	103.54	115.43	118.26
M_y [kNm]	−0.52	0.25	−0.02	−0.23

the steel from the girders. As a result of the tests, the yield strength $\sigma y = 250$ [MPa] was obtained for type A plate girders, and the yield strength σye = 285 [MPa] for type B girders. The obtained results are summarized in Table 7.

4.4 Girder prestressed loaded with the force P

The current section focused on the measurement of the deflection of prestressed girders loaded with the force P. The deflection of the plate girders was measured using a dial indicator mounted on a specially made mounting stand. Three measurements were taken successively for each load. The average results are presented in Figs. 8 and 9. For an unstressed girder, the deflection caused by the critical load on the structure is greater than for prestressed girders, as shown by the measurements of the girder deflection line under load P. Girders prestressed as a result of the process of technological prestressing have an initial rise arrow with convexity upwards. Additionally, loading them with a critical force causes their deflection, but it is so small that even after loading, the structure still has a positive rise arrow.

4.5 Numerical model of girders

The process of constructing a geometric model began with defining points characteristic of the structure in the coordinate system, connecting them with lines, and then superimposing the surface. Next, the boundary conditions were defined. Removing the appropriate degrees of freedom from

Table 7 Internal forces comparison (experimental test vs. analytical model)

	Analytical results				Experimental results			
Girders section	A2	A3	A4	B2	A2	A3	A4	B2
Prestressing forces [kN]	142.69	289.58	439.99	491.25	165.2	303.47	496.14	561.39
Prestressing moments [kNm]	30.31	47.77	72.23	99.34	35.1	50.06	81.45	113.53
Deflection arrow [mm]	2.44	3.73	5.21	3.00	2.90	4.00	6.00	3.50

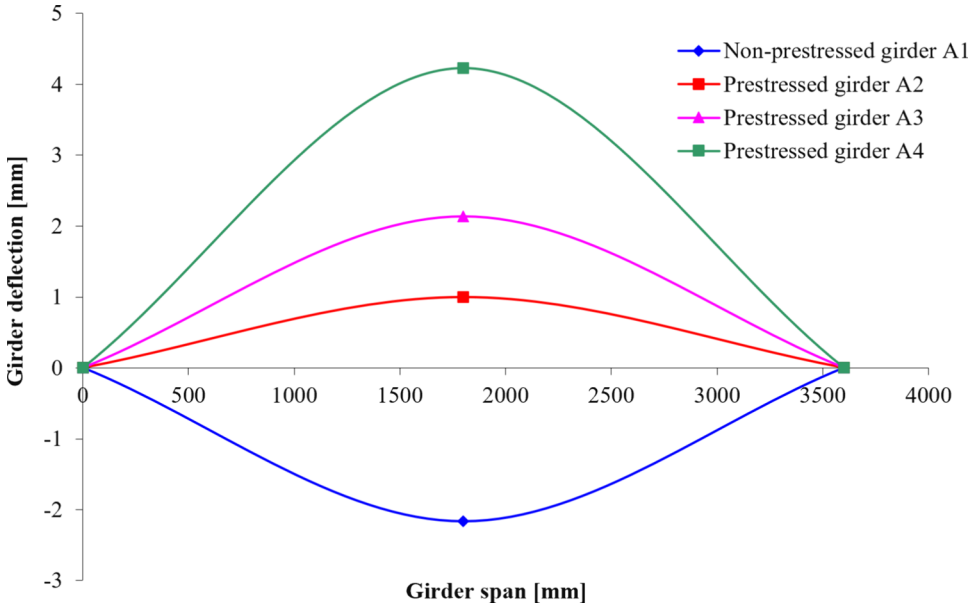

Fig. 8 Deflection variation of girder A under load with force $P = 50$ [kN]

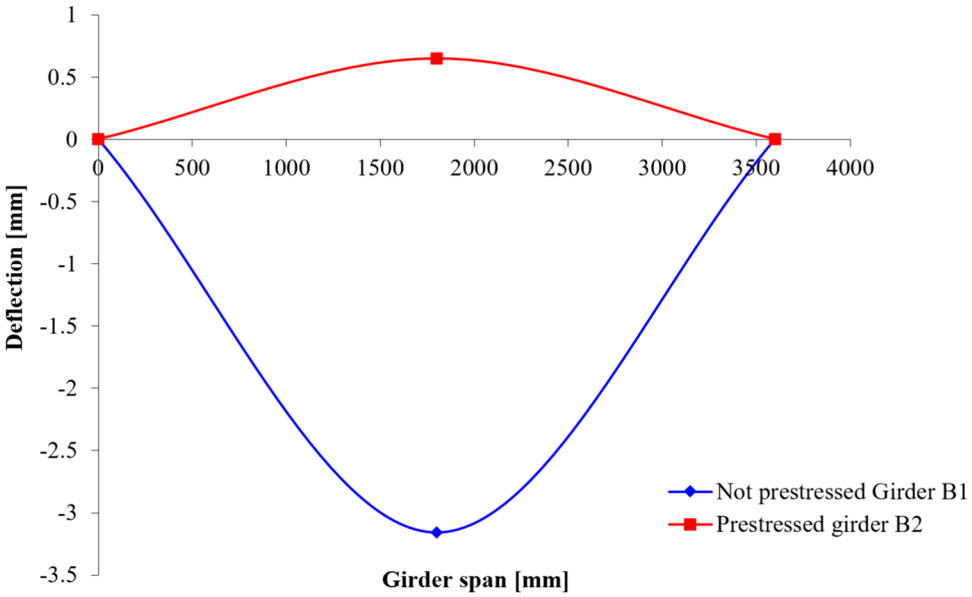

Fig. 9 Deflection variation of girder B under load with force $P = 95$ [kN]

the object determines its behaviour under load, so it should correspond to the actual conditions during the tests.

The girder model was supported as follows: the joint edges of the surfaces of the two highly stiffening ribs with the surfaces of the bottom chords were selected as the elements proper to receive the degrees of freedom. It should be added that in the actual girder, there are elements made of half a Φ 57 × 6.3. The construction of the mesh began with defining the thickness of individual elements. In this case, there are four characteristic thicknesses of finite elements: 4mm thickness—web thickness; rib thickness except for the middle rib, which is 5 mm—thickness of the bottom chord (stretched under live load); and the middle rib, which is 6 mm—thickness of the upper flange (compressed under live load); and 12 mm—thickness of the web part in the location of the prestressing strips. S235 steel was adopted for the ANSYS software. A four-node SHELL 93 shell element was used to discretize the model. The load on the girder is a concentrated force $P = 95$ kN applied to the upper chord through the S24 rail. Since the rail in this work was not made due to large disturbances in the geometry of the model (in the analysis, two types of objects should be taken into account, as the rail cannot be a shell object but a solid one), an equivalent load method that would replace the rail had to be introduced. The girder was therefore loaded by a continuous load acting along the length of the rail.

The welding process was carried out by loading the structure along the weld line at a temperature of 600 °C. In the next step, cooling of the welds was carried out. In order to verify the correctness of the obtained results of the prestressing forces and moments, a numerical analysis of type B girders was carried out. The load was carried out by applying forces to nodes along a length equal to the length of the rail in the experimental model. At the location of the side covers, the thickness was assumed to be equal to the sum of the thickness of the web and two side covers. The welding process was carried out by loading the structure in the place where the welds were laid, with the value of prestressing forces obtained through experimental tests distributed over the length of the weld. Figure 10 shows the stress map of an unstressed girder loaded with the force $P = 95$ [kN], while Fig. 11 shows the stress map of the girder after the technological prestressing process. The results of the numerical analysis were compared with the results obtained through the experimental study. Table 8 indicates the stressed obtained by analytical solution, experimental measurements and numerical FE model in in section D, point 7.

5 Conclusions

The process of replacing girders in structures and construction applications is considered a complex process in addition to its high cost and time-consuming. In recent years, technological prestressing has emerged as one of the effective methods for treating permanent deviations in thin-walled plate girders. In this study, the possibility of applying this method to welded thin-plate S235JRS steel girders was investigated through an analytical and numerical study based on finite elements, and the results were validated experimentally. Seven sensor positions of each girder section (A, B, C, and D). The results indicated:

1 For technological compression, there is a convergence in maximum deflection of 6 mm experimentally and 5.21 mm analytically, both at girder section A4.
2 The temperature distribution on the top weld of the girder increased rapidly up to 90 °C and then decreased smoothly to room temperature.

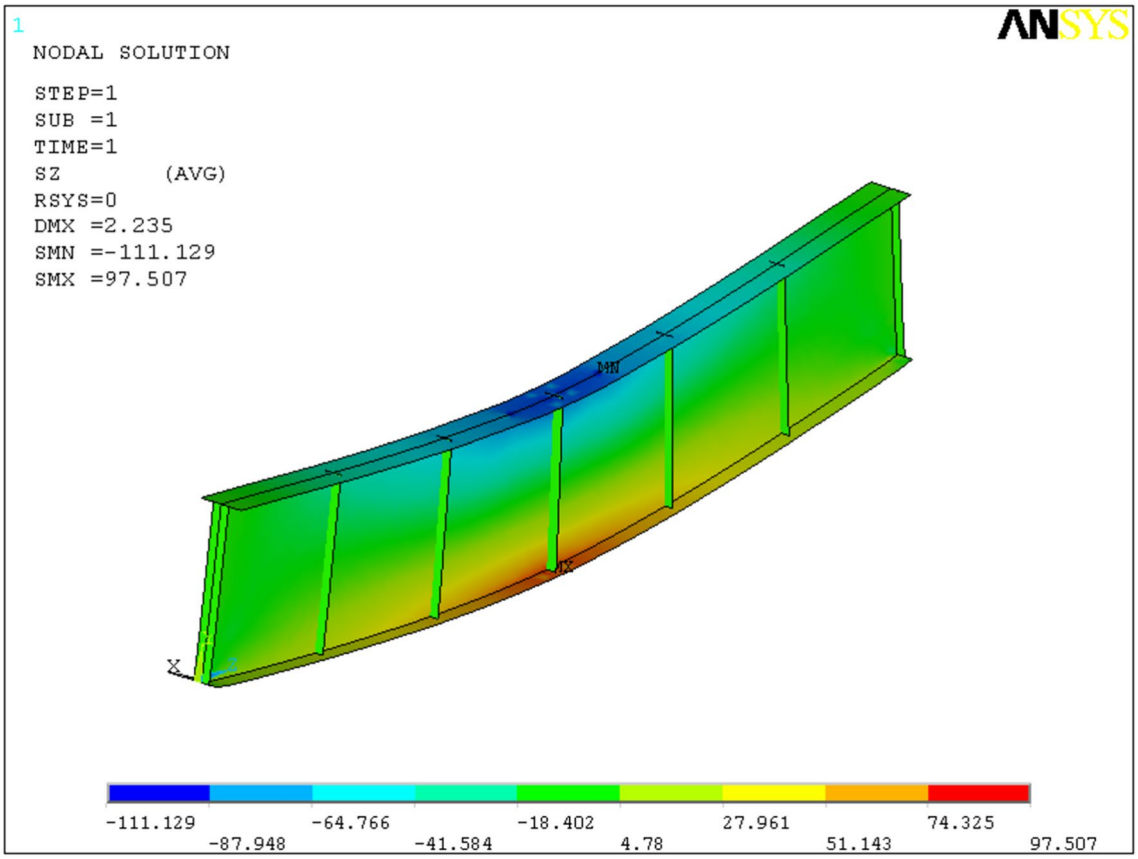

Fig. 10 Stress map of girder B1 loaded with force $P = 95$ [kN]

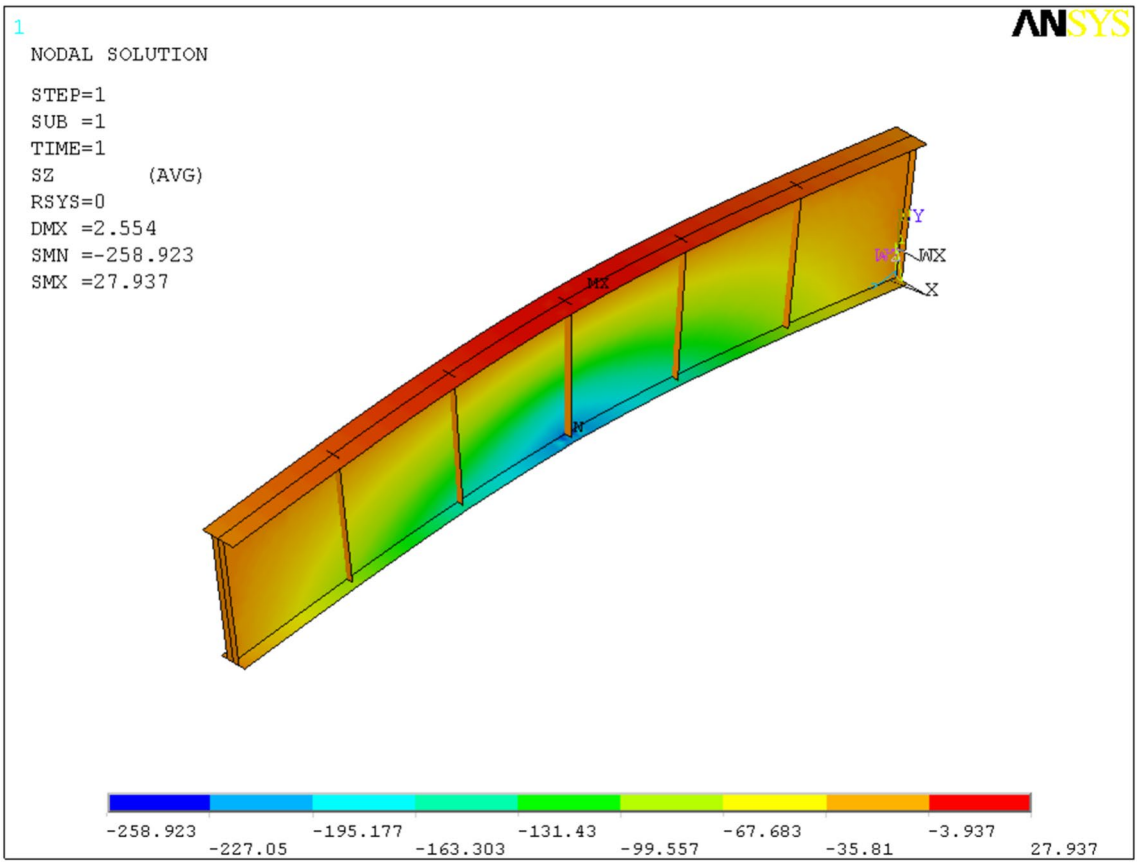

Fig. 11 Girder stress map after technological prestressing

Table 8 Comparison of stresses values obtained by analysis model, experimental measurements and numerical FE

	Calculation results		Experimental results		Numerical Results	
Case	Tension σ [MPa]	Deflection f [mm]	Tension σ [MPa]	Deflection f [mm]	Tension σ [MPa]	Deflection f [mm]
Girder B1 (unstressed)	− 110.01	− 2.65	− 106.81	− 3.16	− 111.13	− 3.10
Girder B2 (prestressed)	30.96	2.50	44.28	3.50	27.93	3.52

3 In the case of loading the girder with constant force, the girder A2 section achieved lower defection, while the maximum values were achieved at the girder A4 section.
4 When compared the girder B1 (unstressed) and girder B2 (prestressed), the girder B1 was in compression while the girder B was in tension.
5 In prestressed girder B, the tensions that were reached were 36.96 MPa, 44.28 MPa, and 27.93 MPa in the analytical, experimental, and FE numerical models, respectively. The corresponding deflections that were reached were 2.50 mm, 3.50 mm, and 3.52 mm, respectively.
6 Regarding the increase in stiffness, prestressing did not significantly increase the inherent stiffness of the beam itself, which aligns with the theoretical understanding that the prestressing procedure primarily affects the stress distribution rather than the structure's stiffness. On other hand, the act of welding extra prestressing strips onto the structure has a significant positive impact. It significantly improves the buckling length of the plate girder's web, thereby enhancing its stability under load.
7 The optimal configuration uses side overlays, which enhance the overall stiffness and achieve the desired effect of levelling deflections without significantly increasing the structure's weight.

Acknowledgements Finally, the authors extend their heartfelt gratitude to the late Prof. Dr. A. F. Blum for his invaluable guidance and advice throughout this study.

Author contributions Raheem Al-Sabur was involved in the investigation, methodology, and writing—original draft. Hassanein I. Khalaf and D. Chodorowska contributed to the investigation, data curation, and writing—original draft. Andrzej Kubit and Wojciech Macek participated in the conceptualization, resources, supervision, and writing—review and editing". All authors have read and agreed to the published version of the manuscript.

Funding No funding was received for conducting this study.

Declarations

Conflict of interest The authors declare no competing interests.

Ethical approval Not applicable.

Consent to participate Not applicable.

Consent for publication All authors of the article consent to publish.

References

1. Pressmair N, Kromoser B (2023) A contribution to resource-efficient construction: design flow and experimental investigation of structurally optimised concrete girders. Eng Struct. https://doi.org/10.1016/j.engstruct.2023.115757
2. Sun Z, Siringoringo DM, Fujino Y (2021) Load-carrying capacity evaluation of girder bridge using moving vehicle. Eng Struct. https://doi.org/10.1016/j.engstruct.2020.111645
3. Liu S, Zhao L, Fang G, Hu C, Ge Y (2021) Investigation on aerodynamic force nonlinear evolution for a central-slotted box girder under torsional vortex-induced vibration. J Fluids Struct. https://doi.org/10.1016/j.jfluidstructs.2021.103380
4. Collins W, Sherman R, Leon R, Connor R (2019) Fracture toughness characterization of high-performance steel for bridge girder applications. J Mater Civil Eng. https://doi.org/10.1061/(asce)mt.1943-5533.0002636
5. Ghanim G, Baldawi W, Ali A (2021) A review of composite steel plate girders with corrugated webs. Eng Technol J https://doi.org/10.30684/etj.v39i12.2193
6. Zheng Z, Liu L, Liu P, Yu Z (2023) Uncertainty analysis of the long-term deformation of crts III slab ballastless track-prestressed concrete simply supported girders. Structures. https://doi.org/10.1016/j.istruc.2023.05.017
7. Zeng P, Wang R, Sun Z, Zhou J (2019) Deflection analysis of long-span girder bridges under vehicle bridge interaction using cellular automaton based traffic microsimulation. Mathematical Biosci Eng. https://doi.org/10.3934/mbe.2019281
8. Bažant ZP, Yu Q, Li G-H (2012) Excessive long-time deflections of prestressed box girders. I: record-span bridge in palau and other paradigms. J Structural Eng. https://doi.org/10.1061/(asce)st.1943-541x.0000487
9. Yamaguchi E, Tsuji H, Tanaka Y (2017) 16.24: Load-carrying capacity of steel girder damaged by collision. ce/papers https://doi.org/10.1002/cepa.481
10. Zhou J, Sun Z, Wei B, Zhang L, Zeng P (2021) Deflection-based multilevel structural condition assessment of long-span prestressed concrete girder bridges using a connected pipe system. Measurement (Lond). https://doi.org/10.1016/j.measurement.2020.108352
11. During O, Malaga K (2014) Life cycle cost analysis on impregnated bridge edge beams. Restor Build Monum. https://doi.org/10.1515/rbm14.20.6-0043
12. Blum, A (1999) Straightening of travelling crane box girders by the method of technological prestressing. VDI Berichte
13. Jia J, Zhang K, Wu S, Xiong T, Bai Y, Li W (2021) Vertical cracking at girder ends during post-tensioning of prefabricated prestress concrete bridge t-girders. Structural Concrete. https://doi.org/10.1002/suco.202100004
14. Pasternak H, Launert B, Kannengießer T, Rhode M (2017) Advanced residual stress assessment of plate girders through welding simulation. In: Proceedings of the procedia engineering 172
15. Blum A, Chodorowska D (2007) Experimental analysis of prestressed thin-walled structures stability. Thin-Walled Structures. https://doi.org/10.1016/j.tws.2007.08.040
16. Hingnekar DR, Vyavahare AY (2022) Steel plate girders behaviour under shear loading. Mater Today Proc. https://doi.org/10.1016/j.matpr.2022.04.173
17. Nascimento S, Santos R, Pedro J.O **(2022)** Behaviour of plate girders with intermediate transverse stiffeners—experimental investigation. ce/papers https://doi.org/10.1002/cepa.1806.
18. Natesh SP, Sarma IV, Baskar K (2018) Tension field action in plate girder under various loading conditions. Int J Civil Eng Technol 9:130–138
19. Shawky W, Nabil G (2018) Experimental and numerical study for the post buckling behaviour of plate girders subjected to bending and shear. In: Proceedings of the MATEC Web of Conferences 162
20. Scandella C, Neuenschwander M, Mosalam KM, Knobloch M, Fontana M (2020) Structural behavior of steel-plate girders in shear: experimental study and review of current design principles. J Structural Eng. https://doi.org/10.1061/(asce)st.1943-541x.0002804
21. Yatima MYM, Azmia MR, Mukhlisinb M (2020) Performance of steel plate girders with inclined stiffeners. Jurnal Kejuruteraan 32:129–137
22. Cakiroglu C, Bekdaş G, Kim S, Geem ZW (2020) Optimisation of shear and lateral-torsional buckling of steel plate girders using meta-heuristic algorithms. Appl Sci (Switzerland). https://doi.org/10.3390/app10103639
23. Alinia MM, Shakiba M, Habashi HR (2009) Shear failure characteristics of steel plate girders. Thin-Walled Structures. https://doi.org/10.1016/j.tws.2009.06.002
24. Okerblom N.O, Matskevich V.D, Bazilevskii N.G, Ronson L.C (1958) The calculations of deformations of welded metal structures